A Metareinforcement-Learning-Based Hyperspectral Image Classification With a Small Sample Set

Prince Yaw Owusu Amoako ⬚, Guo Cao ⬚, *Member, IEEE*, Di Yang ⬚, Lord Amoah ⬚, Yuexuan Wang ⬚, and Qiqiong Yu ⬚

Abstract—The fine spectral information contained in hyperspectral images (HSI) is combined with rich spatial features to provide feature qualities that serve as distinguishing variables for efficient classification performance. The task's objective is to correctly identify and categorize several object categories in the HSI, such as the ground, flora, water, and buildings, based on their spectral characteristics beneficial for a variety of applications, including mapping minerals, analyzing vegetation, and mapping urban land use. The difficulty of learning new task-specific knowledge from a limited data sample that encourages less training has not been overcome by deep learning models. The capacity of current models to generalize to new tasks on small datasets is still lacking. By learning features that are transferable to facilitate adaptation to novel tasks on small samples, metareinforcement learning (Meta-RL) shows promise in overcoming such difficulties. We proposed a Meta-RL model that decouples task inference to improve metatraining and accelerate metalearning with small HSI labeled samples for efficient classification. The model employs a capsule network for effective cooperation between spectra and spatial bands. To minimize the temporal difference error, the Apex-X Deep Q network parameter update is used to metatrain our model. The proposed model obtains an overall accuracy between 95.85% and 96.78% with computational time between 3207.9 and 7487.9 s for training and validation as well as between 21.57 and 32.98 s for testing. The experimental results prove the competitiveness of the proposed model to existing traditional deep learning, metalearning, and reinforcement learning methods in both classification accuracy and computational cost.

Index Terms—Hyperspectral image (HSI), metareinforcement learning (Meta-RL), small sample classification.

I. INTRODUCTION

HYPERSPECTRAL image classification (HSIC) has been very useful in remote sensing in many application fields due to detailed spectral and spatial information produced by the evolving advanced hyperspectral imagers [1]. However, there are limited labeled samples, especially in cross-domain classification problems [2]. The application of the hyperspectral image (HSI) is particularly complicated and challenging because of the nonlinearity of the data and the close association between bands. Particularly, the lack of available hyperspectral training samples makes it difficult to increase classification accuracy. In order to increase classification accuracy, it is therefore necessary to fully utilize the benefits of HSI data by using algorithms and techniques to address the issues of small training sample sizes, high-dimensional HSI data, and effective classification methods [3].

There are negative effects of spectral mixing on pseudolabel generation and classifier training on small data sample classification. To reduce such negative effects, a weakly supervised technique has been employed to use segmentation graphs and neighborhood relationship-based algorithms [4]. A systematic survey of deep learning algorithms employed recently, specifically focusing on research conducted from 2019 upwards on HSIC revealed that scarcity of labeled samples has a major effect on deep learning models' performance [5]. Fully utilizing the rich spatial and spectral details of HSI promotes profound high precision of small data sample classification. In view of this, Li et al. [6] proposed a deep reinforcement learning (RL) technique to process the spectral features, selecting the most informative bands and using extended morphological profiles to extract the spatial features and further classify them with a capsule network. The result of employing RL with a capsule network indicates their appropriateness in HSIC; however, this is satisfactory for retrieving only discriminant and informative target HSI features [7].

Data augmentation is a significant method widely employed as a viable solution to small sample classification problems specifically at the preprocessing stage. Aside from the traditional data augmentation techniques such as rotation, flipping, introducing noise, etc., a number of new methods consisting of CutMix, Cut-out, sample pairing, and unlabeled data utilization have been explored [8], [9]. These methods have realized their effectiveness with sparse data and are, therefore, ineffective and produce low classification accuracy under extremely few available labeled samples [8]. Enhancing data augmentation in the HSIC, Wang et al. [8] proposed a technique with 13 augmentations, including a novel rotation created for HSI patches, that randomly chooses augmentations and their magnitudes

Prince Yaw Owusu Amoako, Guo Cao, Yuexuan Wang, and Qiqiong Yu are with the School of Computer Science and Engineering, Nanjing University of Science and Technology, Nanjing 210094, China (e-mail: papaprince@njust.edu.cn; caoguo@njust.edu.cn; yxwang@njust.edu.cn; yu_qiqiong@163.com).

Di Yang is with the Wyoming Geographic Information Science Center, University of Wyoming, Laramie, WY 82071 USA (e-mail: dyang1@uwyo.edu).

Lord Amoah is with the School of Computer and Software, Nanjing University of Information Science and Technology, Nanjing 210044, China (e-mail: lrdamoah@gmail.com).

for each training iteration. At the start of the preprocessing stage, extended morphological profiles were used after principal component analysis, and affine transformation was introduced as a replacement for all of the geometric augmentations in order to lower the computational cost. A study on CNN models for the HSIC prompted a design of a model to salvage the challenges of high computational power and optimization, Ullah et al. [10] proposed a deep snap smooth wavelet CNN shots ensemble for the multiresolution HSIC with significantly high accuracy specifically solving the optimization problems in ensemble creation to improve the classification performance. These approaches work together to reveal the promise of the HSIC, providing ways to obtain accurate and dependable classification results even with limited training data. However, most of these methods are unable to create local correlations in images as well as make accurate generalizations when there is inadequate data, which is where metareinforcement learning (Meta-RL) shines.

It is realized that most of the existing algorithms based on convolutional neural networks (CNNs) for small data samples in the HSIC have mainly ignored the global spatial information and considered only the local feature information [2]. The limitation of higher accuracy of the HSIC with CNN models is associated with the deficiency of discriminating spectral–spatial features of diverse HSI cubes as well as spatially adjacent categories of spectral similarities [11]. In dealing with the high-level complexity of the HSI spectral–spatial challenge capsule networks have been useful in small sample problems [12], [13], [14], [15]. Paoletti et al. [16] proposed a spectral–spatial capsule model that consists of several building blocks to improve the deep CNN classification accuracy. Improving the extraction competency of deep CNN models on high-level spectral–spatial features, a capsule network is constructed with a residual module for the small sample HSIC [11].

In spite of the significant improvement on the HSIC with capsule networks, they are challenged with parameter redundancy and lack robustness. To mitigate this challenge, Peng et al. [2] proposed a metalearning approach with a convolutional transformer-based for the HSIC. Employing a stack of convolutional blocks, Gao et al. [7] proposed a model with model-agnostic metalearning to enhance the small-sample-based HSIC to provide robustness.

The aforementioned CNN methods and the metalearning methods have improved the HSIC accuracy by addressing significant challenges. However, much is desired to improve the performance in dealing with other challenges such as better band selection and eliminate intractable optimization challenges. An unsupervised deep RL is constructed to select better bands in the HSIC [17]. Feng et al. [18] employed semisupervised deep RL to select optimal bands for the HSIC. Also, a Meta-RL technique that leverages a dynamic structure-aware graph convolutional network for a shared method for value network and policy network is proposed for small sample HSI band selection in a supervised fashion [19].

Meta-RL is pointed out to have the potential of offering improved classification performance by selecting better bands in the HSI if combined with appropriate deep learning frameworks [17]. Since different classes may have variable number of

varying subsets of optimal bands, determining the appropriate band combination for each class is quite challenging, and Mou et al. [17] suggest that a supervised deep RL will be a possible approach to address this challenge. The learning algorithms of the existing deep RL require the method to depend on a large number of interactions with the environment, greatly increasing the training cost with the change of environment [20]. Therefore, the model has to be retrained, learning from scratch since the initially learned optimal strategy is inapplicable in a new environment, which is obviously very inefficient. Li et al. [3] opine that future research on the HSIC will focus on developing appropriate strategies for small samples, which will greatly enhance the application of the HSI in diverse fields.

Hence, Meta-RL is proposed to aid in addressing such challenges on the HSIC with small data samples. To the best of our knowledge, this is the first time implementing Meta-RL incorporating capsule network and Q-learning for the HSIC. This article proposes a Meta-RL for the small sample HSIC with the following significant contributions.

1) Employing a capsule network to capture the specific HSI feature bands and obtain underlying spatial hierarchical relationships between these bands to enhance classification performance.
2) A more robust and stable Meta-RL method that can achieve effective corporation among HSI features with a minimal convergence period to improve HSI small sample classification problems. This provides a direction for further research on the small sample HSIC with Meta-RL.
3) Detailed experimental evaluation on four Chinese HSI datasets in comparison with recent state-of-the-art traditional deep learning models, metalearning models, and Meta-RL models on performance accuracy and computational complexity.

The rest of this article is organized as follows. We discuss related work in Section II, and the proposed method is presented in Section III. In Section IV, we introduce the experimental setup and preliminary evaluation of the method. The evaluation of our method in comparison with existing methods is discussed in Section V. Finally, Section VI concludes this article.

II. RELATED WORK

A. Metalearning

Metalearning, also known as "learning to learn," focuses on training models to learn from multiple related tasks in order to improve their generalization capabilities. Instead of training a model on a single task, metalearning involves training it on a distribution of tasks sampled from a larger task space. The goal is to acquire knowledge and adapt quickly to new, unseen tasks using a few data samples. In supervised and semisupervised HSI detection and classification with deep learning in which considerable retraining for generation in an unknown application context, the metalearning approach is realized to be promising.

In view of this Wang et al. [21] introduced a metalearning model with Siamese CNN for HSI detection. Zhou et al. [22] proposed a metalearning method for the small sample HSIC

using an embedding module and a linear classifier as a backbone classification framework. Recent work on few-shot HSIC considering the challenge of open-set recognition is a metalearning model based on the generative adversarial network [23]. Liang et al. [24] addressing the unseen aspect category of small data samples for effective sentiment analysis, proposed an aspect-focused episode-based metalearning model to learn to generalize new aspects. A metalearning approach is introduced to address the limited labeled samples of the target domain in the HSIC [2]. The method basically employs a convolutional transformer that uses small data sample to extract local-global features and further introduces a domain discriminator to reduce domain shift as well as distinguishing the source of each domain feature.

There exist a significant number of benefits in the implementation of metalearning including improving machine learning models and adaptation to new tasks with fewer samples. However, the time required to metalearn is considerably long [25]. There is a need to fill the long-time execution of metalearning in research on the HSIC by enhancing the learning process to be rapid.

B. Reinforcement Learning (RL)

RL is a type of machine learning where a model interacts with an environment and learns to take actions to maximize a cumulative reward signal. The model learns through trial and error by receiving feedback (rewards) from the environment based on its actions. The objective is to find a policy that maps states to actions, optimizing for long-term rewards. RL is employed to demonstrate an effective and efficient hyperspectral band selection [18]. The model constructed a semisupervised CNN introducing intraclass compactness constraint with sufficient unlabeled samples and small labeled samples. An unsupervised deep RL model is proposed to select bands for the HSIC [18]. The model considers HSI band selection as a Markov decision process and builds an RL model that can intelligently select optimal bands through learning policy with no hand engineering. Fu and Zhang [26] proposed a plug-and-play model based on RL for HSI reconstruction to balance spatial and spectral resolutions. The model's parameters can be adaptively tuned to change the denoising strength, the deep denoising network's penalty factor, and the iterative optimization's terminal time using a suitable policy network trained using deep RL. Although band selection methods are improving the HSIC process, the current RL-based methods require large amounts of samples to learn and lack the generalization ability to a new environment.

A survey conducted on brain-inspired algorithms employed on remote sensing data interpretation revealed that through interaction with the environment, RL in remote sensing chooses consecutive actions by maximizing cumulative feature rewards. RL can achieve relatively high accuracy without utilizing any labeled training dataset, especially when there are only a few labeled pixels available [27]. The classification of polarimetric synthetic aperture radar images was proposed using an improved

deep Q-network (DQN) algorithm for few-shot remote sensing data. By interacting with models in a greedy way, it can produce useful data [28]. In the network, environment states and model actions are used to refer to multilayer feature images and classification operations, respectively. Model predictions are rewarded under some circumstances.

A small sample set of data that has been annotated is used to provide feedback to the model. The aforementioned models establish the usefulness of RL in HSIC tasks, nonetheless, the inherent challenges of sample inefficiency and exploration for RL training requires metatraining with better models such as capsule network to improve the training efficiency.

C. Metareinforcement Learning (Meta-RL)

Meta-RL on small sample data classification seems promising in solving the fast adaptation on novel tasks. Nonetheless, their capabilities are generally limited to narrow task distributions, even though the main objective of Meta-RL is to aid in the rapid acquisition of completely new characteristics. A survey of Meta-RL [29] indicated the need for future research to focus on Meta-RL on small sample data classification models feasible for the generalization of broader task distributions. They further proposed that a simple way to achieve such an objective is to perform metatraining that learns an inductive bias enhancing generalizability on a wider task distribution. Existing models have limitations on exploration in training on a wider task distribution and the agent may face challenges on test tasks that are beyond the training distribution. Generalization is very significant in an environment of such an out-of-distribution because a Meta-RL method usually faces unexpected tasks in practical implementations.

This article seeks to take advantage of the existing rich labeled HSI dataset enough for training a Meta-RL model, and then, subject it to a novel HSI dataset for new task distribution classification.

To improve the effectiveness of band selection in the HSI by addressing the challenge of existing models leaving inherent correlation and common knowledge in varying bands, Feng et al. [19] proposed a Meta-RL technique for zero-shot band selection of hyperspectral features. A survey of metalearning with its incorporation of RL revealed the significance of their application in small data sample implementations in many fields [30].

It is realized that most existing Meta-RL techniques infer the task objective from the new task environmental reward function, which is impracticable in many practical applications. A Meta-RL approach for rapid policy adaptation incorporating preference-based feedback is developed to bridge such gap [31]. The challenge in the existing Meta-RL remains that they take a longer time to converge with performance instability. A more robust and stable Meta-RL method that can achieve effective corporation among HSI features with minimal convergence period is required to improve HSI small sample classification problems. Inspired by [32], the problem of Meta-RL for the HSI small sample classification is defined in the following.
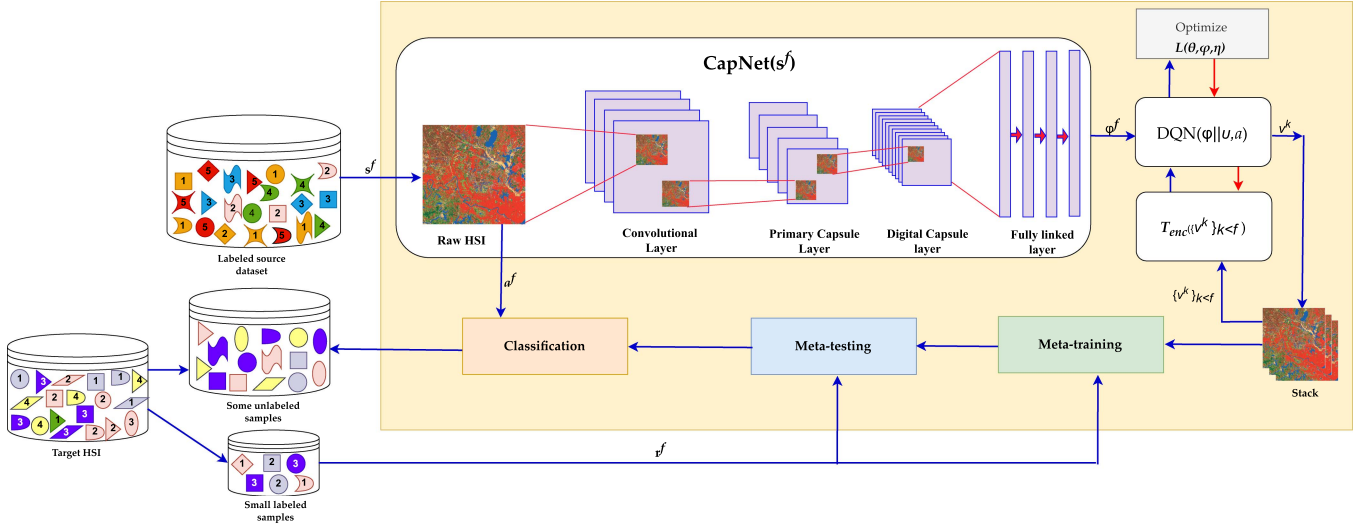
Fig. 1.   Architectural framework for the proposed Meta-RL for the small sample HSIC.

The spectra-spatial feature extraction as a metatask. Given a k-set metatraining task (consisting of different HSIs) $\mathcal{H}_{\text{meta}} = \mathcal{H}_1, \ldots, \mathcal{H}_k$, a feature extraction policy capable of fast learning a new task is to be learned. In simple terms, the policy for metalearning can effectively adapt to learning spectra-spatial features of new sets of HSIs with varying conditions. Hence, the Meta-RL, given a metatraining loss function $\mathcal{L}$, parameter representing the policy for solving a task $\mathcal{H}_i$ as θ_i, based on the Meta-RL algorithm is formulated as

$$\theta_{\text{meta}} = \underset{\theta}{\arg\min} \frac{1}{k} \sum_{i=1}^{k} \mathcal{L}\left(\theta_i\,\mathcal{H}_i\right), \theta_i = \Re_\theta\left(\mathcal{H}_i\right). \quad (1)$$

We assume that each model deals with a single image at a time and the metatraining task $\mathcal{H}_i$ is expressed as a Markov decision process with $\{\mathcal{S}_i, \mathcal{A}_i, \mathcal{P}_i, r_i, \pi_i, \lambda_i\}$ elaborated as follows.

1) $\mathcal{S}_i$ is the state space, where $s_i^f \in \mathcal{S}_i$ represents the raw observation of the model i at point f, which comprises the current phase of feature and the number of spectra–spatial features of images i.
2) $\mathcal{A}_i$ is the action space. $a_i^f \in \mathcal{A}_i$ representing the selected action of model i at point f. The model's selection is at every change of point Δ_f from its activated predefined phase.
3) $\mathcal{P}_i$ is the transition probability given by $\text{P}(s_i^{f+1}|s_i^f, a_i^f)$ representing the probability of arriving at the state s_i^{f+1} given the state s_i^f and the action a_i^f.
4) r_i is the reward, which r_i^f defines as the negative value of the sum of the spectral and spatial features of an image i at point f.
5) π_i is the policy for feature extraction and λ_i is the discount factor. The model's goal is to learn the optimal selection strategy given by $\pi_i\left(a_i|s_i\right)$ to minimize the total expected reward expressed as $\mathbb{E}[\Sigma_{f=1}^{\varepsilon}(\lambda_i)^f r_i^f]$, where $\mathbb{E}$ denotes the number of episodes.

Fig. 1 depicts the architectural framework for Meta-RL for classifying the HSI with a small sample set.

III. PROPOSED METHOD

The proposed Meta-RL model for the HSI small sample classification is composed of three parts: the capsule network (CapsNet, parameterized as η), task encoder (T_{enc}, parameterized as φ), and the policy learner (DQN parameterized as θ). The CapsNet learns the adjacent HSI feature bands, whereas the T_{enc} makes an inference of the task properties from the spatial and spectral bands, and the DQN makes decision based on the current state and the task inference output by the T_{enc}.

A. Capsule Network

A novel deep learning architecture called the capsule network [33] aims to get over CNNs' drawbacks, such as the absence of explicit entity ideas and the loss of important data during the Max-pooling. The underlying relationships between the features are also captured via a capsule-based representation approach. As a result, in this situation, the capsule network performs well with fewer training samples and is more resistant to affine changes. This is evident in the HSIC result obtained in [33]. Hence, its adoption in this research. We employ a typical capsule network with a multilayer capsule system that has the ability to distinguish between objects while being trained.

A convolutional layer, a primary capsule layer, a digital capsule layer, and a fully linked layer are the four component pieces in our model. The capsule creates a vector output from the input data. The probability of the vector's existence is shown by its length, and its attribute is indicated by its direction. Following the concept in [34], the network's -linear squashing function determines the output vector of capsule k, given by

$$v_k = \frac{\|s_k\|^2}{\epsilon + \|s_k\|^2} \frac{s_k}{\|s_k\|} \quad (2)$$

where ϵ denotes a fixed size determined value, and s_k can be deduced as

$$s_k = \sum_i c_{ik} W_{ik} u_i \quad (3)$$

where u_i represents the previous layer output, W_{ik} denotes the prediction vector weights of next layer capsule, and c_{ik} denotes the coefficient determined by the dynamic routing process given as

$$c_{ik} = \frac{\exp(b_{ik})}{\sum_n \exp(b_{in})} \quad (4)$$

where b_{ik} represents the long prior probability that capsule i should be coupled to capsule k. The iteration process fulfills the dynamic routing. A lower level capsule sends its output to a higher level capsule with a larger scalar product between the output vector of the higher level capsule and the input vector of the lower level capsule. The marginal loss $\mathcal{L}_k$ of the capsule k can be defined as [33]

$$\mathcal{L}_k = \mathcal{T}_k \max(0, m^+ - \|v_k\|)^2 + \lambda(1 - \mathcal{T}_k)$$
$$\max(0, \|v_k\| - m^-)^2 \quad (5)$$

where $m^+ = 0.9$, $m^- = 0.1$ denotes default free parameters, λ is a parameter guaranteeing the final convergence, and $\mathcal{T}_k = 1$ if the kth class data are recognized, otherwise $\mathcal{T}_k = 0$.

B. Task Encoder

The task encoder T_{enc} infers the task properties from the HSI spatial and spectral bandsconsidered as constituting spatial and spectral information signified as: $v^f = (\varphi^f, a^f, r^f, \varphi^{f+1})$, where $\varphi^f = \text{CapsNet}(s)$ representing the embedded vector transformation from the raw state s by CapsNet, combining the spatial and spectral bands of different classes to aid the model's corporation. We make the assumption that $\{v^k\}_{(k<f)} = (v^{f-K}, \ldots, v^{f-1})$ representing all the past K transitions until f. The key information about the task construction must be encoded from the inference of the task properties of the latent features as u. The design of the task encoder embeds the feature bands $\{v^k\}_{k<f}$ into the latent features u formulated as

$$u^f = T_{\text{enc}}\left(\{v^k\}_{k<f}\right)$$
$$= T_{\text{enc}}\left(\{(\varphi^k, a^k, r^k, \varphi^{k+1})\}_{k<f}\right). \quad (6)$$

The design of our task encoder network T_{enc} requires to consider the following two main principles.

1) The HSI data constitute complex spatial-temporal patterns. The spatial relationship among the varying image features is captured by the CapsNet and the temporal information about the task are critical for the model. Therefore, the T_{enc} is made expressive enough to capture the temporal information.
2) The T_{enc} should be easily trained to enhance the efficiency of the metatraining, eliminating computational complexities. The gated recurrent unit capable of balancing rich temporal representation and computational complexity is employed to construct the T_{enc}.

The model workflow is then established as follows.

1) At each episode f, the model receives the raw state s^f as input.

2) The CapsNet transforms s^f into corresponding φ^f, which includes information about the target feature and the neighboring feature of the HSIs.
3) Previous K spectral–spatial features are sampled from the stack and fed to the T_{enc}.
4) T_{enc} then generate the latent feature bands u and fed into the DQN to make decision based on s^f and u.

C. Metatraining

The model gains knowledge from a variety of tasks that are each represented by a small labeled HSI dataset during the metatraining phase. The model is given different jobs to perform, and throughout each one, it learns how to adapt and generalize using only a small amount of data. The metalearner is able to learn how to quickly adapt to new tasks with just a few instances since it captures common information across tasks. The current Meta-RL techniques struggle with slow adaption speeds [35] and large computational training complexity [30]. In order to achieve effective performance over all metaparameters (η_{meta}, φ_{meta}, and θ_{meta}), a simple multitask training strategy is used.

The training method, which completes one training at a time for each task, reduces the average reward across all metatraining tasks. Each task is trained across a number of episodes in order to determine the optimal performance metrics for the subsequent task initialization metrics. The final task completed at the conclusion of training results in the metaparameters, which show that the model extracts the experience from all metatraining tasks. As demonstrated in this research, even though our training method is straightforward and simple to use, nevertheless, it outperforms more complex methods currently in use.

Inspired by [32], [36], and [37], our metatraining is performed using Ape-X DQNs method parameters update. The DQN employs a neural network to approximate Q values and tries to minimize the temporal difference error expressed as

$$\mathcal{L}(\theta, \varphi, \eta) = \frac{1}{|\mathcal{B}|} \sum_{(\varphi^f, a^f, r^f, \varphi^{f+1}) \in \mathcal{B}} (r^f + \lambda \max \mathcal{Q}_\theta$$
$$(\varphi^{f+1}\|v^{f+1}, a') - \mathcal{Q}_\theta(\varphi^f\|v^f, a^f t))^2 \quad (7)$$

where $(\varphi^f, a^f, r^f, \varphi^{f+1})$ represents transition sampled from minibatch $\mathcal{B}$ and $\varphi\|u$ represents the concatenation of the embedded state φ and the task inference u. Furthermore, stochastic gradient descent is used to update the parameters of the policy as well as the task encoder given by

$$\theta \leftarrow \theta - \alpha\nabla_\theta \mathcal{L}(\theta, \varphi, \eta) \quad (8)$$
$$\varphi \leftarrow \varphi - \beta\nabla_\varphi \mathcal{L}(\theta, \varphi, \eta) \quad (9)$$
$$\eta \leftarrow \eta - \gamma\nabla_\eta \mathcal{L}(\theta, \varphi, \eta). \quad (10)$$

The metatraining is able to aid the model learn the spectral–spatial features of the HSI for small sample classification.

A layer-wise input–output features is detailed as follows.

1) *Input capsule:* Several HSI feature bands are the input for the capsule network. An HSI various aspects or characteristics are represented by each band, which include infrared bands, color channels, or other pertinent properties.

2) *Primary capsule:* The main capsule layer encodes information such as edges, textures, or color patterns unique to each feature band by processing each HSI feature band independently and capturing low-level properties unique to that band.

3) *Routing by agreement*: The network learns how features in one band relate to characteristics in another, capturing spatial and hierarchical relationships. The dynamic routing method is used to connect capsules in various feature bands.

4) *Secondary capsules:* Higher level features and the connections between feature bands are represented by secondary capsules, which receive their input from the routing mechanism's output. These capsules are useful for capturing more ethereal associations, like the blending of one band's color pattern with another's texture pattern.

5) *Class capsules*: Depending on the relationships that the network has learned between the various bands of HSI features, the final layer of capsules represents particular classes or categories. Each class capsule encodes information about the presence of particular features in combination across the bands, enabling the network to carry out HSIC.

D. Metatesting

The metalearner is assessed on new HSI images for the classification task when the metatraining is completed. A small number of HSI training samples from the new task are used by the model during metatesting to adjust its parameters to the particular task. The objective is to evaluate the model's generalizability and performance on HSI tasks that were not included in the metatraining phase. In this article, forward propagation of the CapsNet Meta-RL model is used to update the model by collecting transitions. To ensure that the CapsNet learns the spatial features due to the varied feature arrangement of the HSIs, and to retrain the CapsNet to properly adapt to the new work environment, the update is solely applied to the DQN and the CapsNet. On the premise that common structures of metatraining tasks are learned and inferences are drawn from task attributes, the task encoder did not require retraining following the idea in [32].

Following the architecture in Fig. 1, Algorithm 1 elaborate on the processes of the model.

Algorithm 1: Meta-RL HSIC.

  Part 1: Metatraining
Input: HSI labeled source dataset, Target HSI
Output: Classified HSI
1:   Input raw HSI into initial capsule
2:   **while** Capsule layer $\neq$ last fully inked layer capsule **do**
3:     Extract low-level features by primary capsule layer $\leftarrow$ CapsNet(s^f)
4:     Extract high-level features through dynamic routing by upper capsule layers $\leftarrow$ CapsNet(s^f)
5:     Reconstruct the input image from the capsule's output
6:     Return relevant features φ^f
7:   **end while**
8:   **do**
9:     Infer task properties from HSI features by T_{enc} using (6)
10:    Initialize parameters
11:    $\eta \leftarrow$ feature bands
12:    $\varphi \leftarrow$ spatial and spectral bands of task properties
13:    $\theta \leftarrow$ Current state and the task inference output
14:    Approximate $\mathcal{Q}$ values using (7)
15:    Update policy parameter using (8)
16:    Update task encoder parameter using (9)
  Part 2: Metatesting
Input: HSI unlabeled samples, HSI small labeled samples
17:    **while** Capsule layer $\neq$ final capsule
18:     Extract low-level features by primary capsule layer CapsNet(s^f)
19:     Extract high-level features through dynamic routing by upper capsule layers CapsNet(s^f)
20:     Reconstruct the input image from the capsule's output
21:     Return relevant features φ
22:    **end while**
23:    Update CapsNet by forward propagation with transitions
24:    Update DQN
25:    **while** final episode not completed
26:    Return classified HSI

IV. EXPERIMENTAL SETUP AND PRELIMINARY EVALUATION

This section establishes the evaluation parameters for the proposed model. The focus is to realize how the model is capable of achieving better classification accuracy and computational efficiency on the small sample HSI through Meta-RL.

A. Setting up the Experimental Datasets and Processes

Recent remote sensing data from satellites have contributed immensely to obtaining rich image resources for the HSIC. This study employs the four HSI datasets with rich spatial and spectral information, the Huan Jing-1 Hyperspectral Image (HJ-1 A HSI), the Gaofen-5 Advanced Hyperspectral Image (GF-5 AHSI), the Zhuhai-1 Orbita Hyperspectral Satellites (OHS HSI), and the Ziyuan-1 02D Hyperspectral Image (ZY-1 02D HIS). Table I presents general background specifications of the sensors for the datasets.

Furthermore, a brief description of the datasets is presented for more clarity as follows.

1) The HJ-1 A/B data are attained from the website of the China Centre for Resources Satellite Data and Application (CRESDA). The images are considered level-2 products, which is obtained after a systematic geometric calibration. The HJ-1 A satellite was on September 6, 2008, covers

TABLE I
GENERAL BACKGROUND SPECIFICATIONS OF THE DATASET SENSORS

Sensor	HJ-1A HSI	GF-5 AHSI	OHS HSI	ZY-1 02D HSI
Year	2008	2018	2018	2019
Altitude(km)	649	705	500	-
Spectral range(μm)	0.45–0.95	0.4–2.5	0.41–1.11	0.4–2.5
Spectral resolution (nm)	5	10-May	2.5	20-Oct
Spatial resolution (m)	100	30	10	30
Bands	115	330	32	166
Swath width (km)	50	60	150	60
Satellite net	Yes	No	Yes	Yes

115 spectral bands with a range of 0.45–0.95 μm. It is indicated that the HJ-1 A hyperspectral imager is able to revisit a single area on earth every 4 days in a solar synchronous orbit [38]. Applications of HJ-1 A hyperspectral data include crop phenology mapping, determination of chlorophyll concentration in water, and other water and agricultural applications [39].

2) The GF-5 HSI data represent the first comprehensive hyperspectral data with a spatial resolution of 30 m from a Chinese observation satellite. There are two land imagers with four atmospheric sounders composed in six payloads of the GF-5 having a full spectral range coverage of land and atmosphere simultaneously. A scene is chosen from HSI data produced by the infrared hyperspectral camera for visible short waves. After atmospheric and radiation correction, from the original data, the range of visible light to near-infrared spectrum is selected. The image size is 200 x 200 with the scene covering 150 spectral bands within the range of 0.4–2.5 μm. The data constituting six ground-truth classes consist of 2 216 labeled samples. The data were retrieved from the CRESDA.

3) The Zhuhai Orbita Aerospace Science and Technology Company Limited (Orbita) designed the OHS dataset. On April 26, 2018, the first set of four OHSs was launched, and September 19, 2019, dated the second batch. There are eight satellites in the Orbita hyperspectral remote sensing satellite constellation network in China with a strong capacity to obtain hyperspectral remote sensing data. It is indicated that each of the OHS satellites' orbits is sun-synchronous at 500-km mean altitude with 98° inclination and has a lifespan of more than 5 years. A dual-frequency Global Navigation Satellite System receiver measures each OHS satellite's position in its orbit, having the support of the global positioning system (GPS) and Beidu, with a combined constellation revisit of 5 days [40].

4) According to [41], the ZY-1-02D satellite is the first civilian service hyperspectral. It was launched on September 12, 2019, and composed of two payload types, an advanced hyperspectral imager sensor and a visible and near-infrared camera. The real Zi Yuan (ZY)-1-02D HSI data was obtained on December 5, 2019. It has an image size of 1400 x 900 x 166 with a spatial resolution of 30 m and 166 bands. Upon preprocessing, 137 bands were used due to the elimination of uncalibrated and noisy bands. The spatial registration of the ZY-1-02D image was done by employing the GF-5 data as the reference image.

In each of the datasets for training and testing, a random splitting of each class was adopted in a ratio of 70% training and 30% testing. All the images were initially resized to obtain 256 × 256 identical sizes and employed CapsNet to directly extract the features. Each image feature dimension remained as 512 × 8 × 8 producing a total of 32 768.

On the experimental processes, all the algorithmic procedures were constructed and implemented using Python with accompanying libraries running on a laptop computer with Intel(R) Core(TM) i7-9750H CPU at 2.60 GHz, 16.0-GB RAM, 64-bit operating system with x64-based processor and NVIDIA GEFORCE GTX. Initially, the learning rate and iterations were varied (from 0.01 and 100, respectively) to ascertain a balanced training pattern which confirmed 0.001 and 2000 as feasible learning rates and iterations, respectively. Generally, we employed hyperparameter settings as 128 parallel actors and batch size, exploration parameters ranging from 0.03 to 0.4, s discount factor of 0.002–0.5, and a learning rate for the Q-network of 0.002–0.5 with an update interval of five episodes. The steps per environment update were considered to be 4 with model save interval at every ten epochs.

B. Preliminary Evaluation of Meta-RL Model for the HSI Small Sample Set

We evaluate the model on the four datasets to determine the accuracy of small data samples with varying epochs and different number of training samples. To train our proposed model, we choose 100 epochs, a patch size of 7 x 7, and a convolution kernel size of 1 x 1 as hyperparameters. Fig. 3 displays the training curves, which are made up of test loss and test accuracy. Fig. 2 depicts the outcome of the model's performance on different number of training samples.

It is revealed that the model generally produces better performance on all four datasets. On the HJ-1 A HSI, GF-5 AHSI, and OHS HSI, the loss was stable after the 80th epoch as compared to the ZY-1 02D, which stabilized after the 50th epoch, although a considerably low loss was obtained on all the datasets. This may be due to the rich information in all the HSI and the capability of Meta-RL to overcome the nonlinearity of the data and the close association among bands even under small training samples.

The high accuracy result with the accompanying less loss produced by our model on all the datasets also indicates that our model can function well in classifying HSI and has the potential to do well even in cross-domain environments with small data samples under supervised learning. The model is,
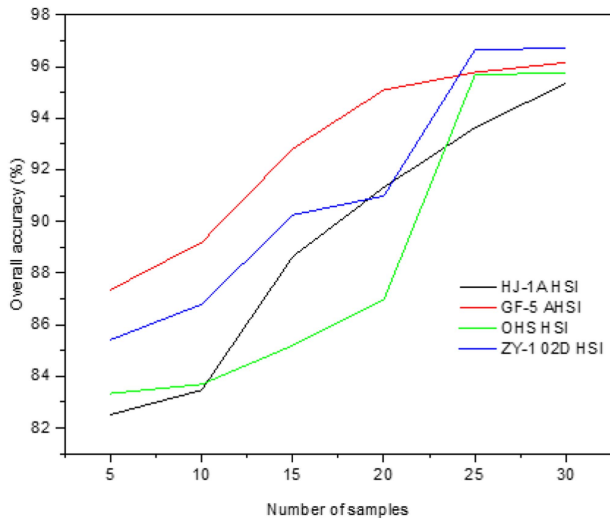
Fig. 2. OA of the proposed model on different training data samples on datasets.

therefore, evaluated on varying data samples to ascertain its effectiveness on small data samples. The performance on each dataset in reference to a varying number of training samples is presented in Fig. 2.

It can be inferred that the model performs steadily well on the GF-5 AHSI dataset, however, the highest accuracy result is obtained on the ZY-1 02D HSI when the sample size is beyond 20. The performance pattern on GF-5 AHSI and the HJ-1 A HSI are quite similar, while that of OHS HSI follows a similar pattern with ZY-1 02D HIS, nonetheless, the model performs quite lower on the OHS HSI. These similarities may be as a result of the similarities in feature patterns among all the datasets. We, therefore, benchmark our model with existing state-of-the-art techniques that have common implementation algorithmic techniques presented in Section V.

V. ABLATION STUDY OF CLASSIFICATION PERFORMANCE ON THE DATASETS

Aiming at evaluating the model's classification performance on the HJ-1 A, GF-5, OHS, and ZY-1 02D datasets on small sample HSIC, the ablation study is conducted with traditional CNN methods, metalearning methods, and metareinforcement methods. The comparison uses three measurement scales: overall accuracy (OA) and average accuracy (AA), which are expressed as percentages, and the Matthew correlation coefficient (MCC), which is expressed as an absolute value. The MCC is a contingency matrix approach to generating the Pearson product moment correlation coefficient for finding the difference between anticipated and actual values [42]. It is claimed to be extremely suitable for classification problems relating to unbalanced datasets. A bold typeface is used to denote the top outcomes for each metric reported in the tests, and the average results are presented. Ten tests are run on each of these to rule out any results that might be unstable owing to random selection during metatraining [43], and the average results are then recorded.

A. Experimental Evaluation of HSIC Performance on Deep CNN Methods

Six existing traditional deep CNN learning methods for the HSIC are compared with the Meta-RL model. The comparison considered three methods that are based on CNN variance, including Deep Cube CNN with random forest (DCNR) for HSIC [44]. A spatial–spectral split attention residual networks (S^{3}ARN) for the HSIC fusing features extracted from multireceptive fields using split attention strategy consisting of bottleneck residual blocks [44]. Multimodal attention-aware CNNs for the classification of hyperspectral and LiDAR data [45] (referred to in this article as MAACNN). Since our model incorporates a capsule network, we compared it with three capsule network-based methods. Capsule networks for the HSIC, which builds on Hinton's capsule network for a CNN model extension in refining capsule unit concept as spectral–spatial units [16] (referred in this article as CapsCNN). Cascade residual capsule network for the HSIC (CRCN) employs residual module to address the spectral similarity of HSI cubes of adjacent spatial categories and capsule network for objects spatial context orientation representation characterization [11]. A multiscale residual capsule network for the HSIC with small training samples (referred: MR-CapsNet) [33].

Second, our model is compared with metalearning-based state-of-the-art methods to investigate the performance in realizing the superiority of fusing metalearning with RL over only metalearning: using model-agnostic metalearning (MAML) with a CNN for small sample HSIC that deals with the classification of cross-data small samples on the same HSI and cross-scene small samples among varying HSI [7]; a spectral–spatial distribution consistent (SSDC) network based on metalearning for the cross-domain HSIC [46]; a Bayesian (BMFSC) perspective that considers the HSI few-shot classification task as a hierarchical probabilistic inference and gives a thorough metalearning probabilistic inference procedure [47]; a cross-domain few-shot HSIC system based on causal metatransfer learning (CMTL) combines causal learning, metalearning, and transfer learning [48]; metatransfer learning for few-shot HSIC (referred in this article as MTL), which builds a linear classifier and an embedding module-based classification model [22]; and convolutional transformer-based few-shot learning for cross-domain HSIC (CTFSL) addresses the problem of small sample learning in a metalearning paradigm [2] .

We finally compare with two RL with no metalearning and Meta-RL methods. Deep RL for band selection in the HSIC (referred in this article as DRLBS) [17], and deep RL forsemisupervised hyperspectral band selection (represented as RLSBS-A) [18]. MR-Selection: A Meta-RL approach for zero-shot hyperspectral band selection (referred in this article as MRS) is considered for the HSIC [19].

Generally, deep CNN models perform well in classifying the HSI as a result of their effectiveness in directly extracting high-level features [44]. The rich features of the datasets used have contributed to the significant performance of the evaluated models in this study, which can be realized in Table II and Figs. 4–7. It can be observed that the deep CNN algorithms that
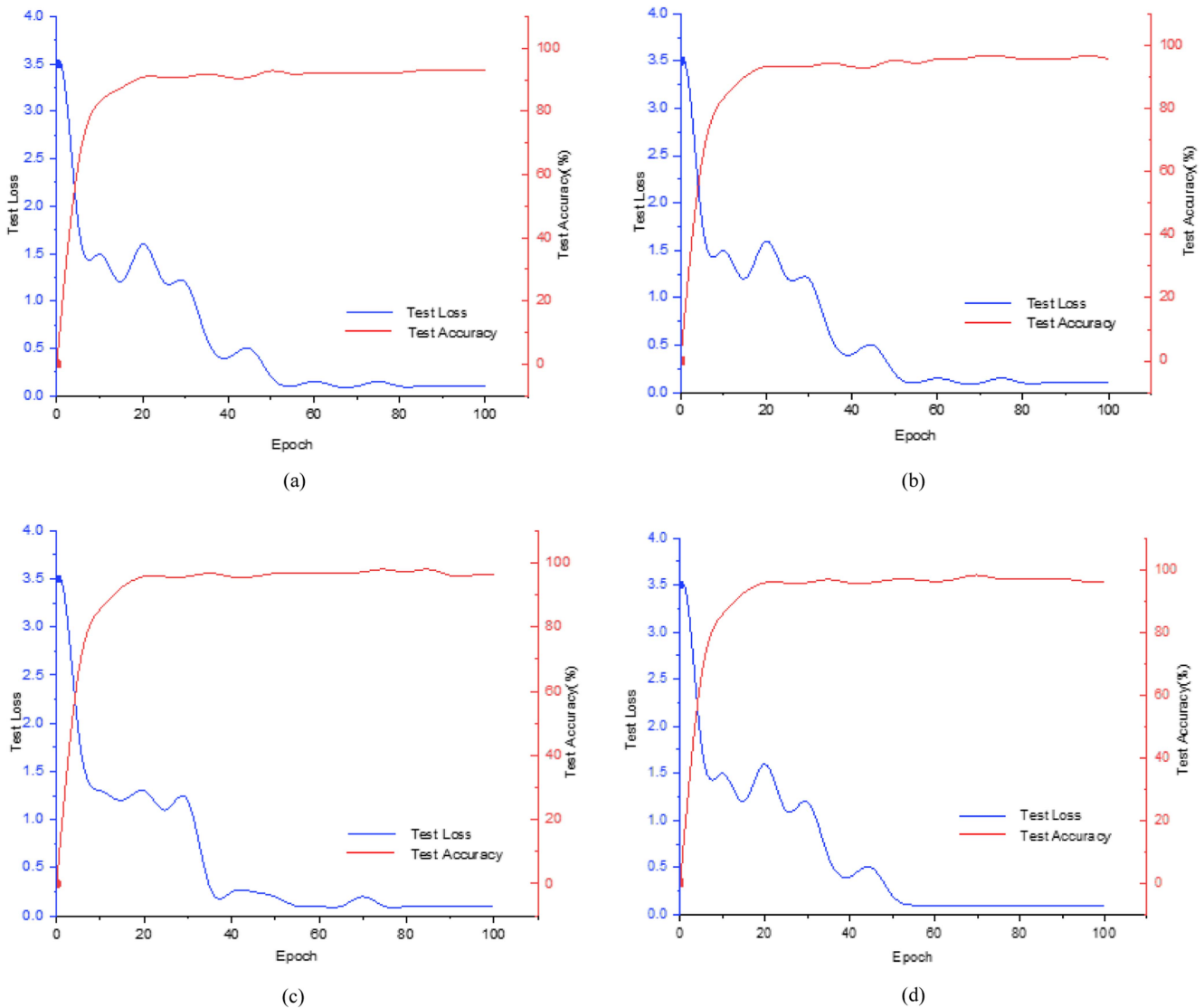
Fig. 3.   Test loss and test accuracy of proposed method on datasets. (a) HJ-1A. (b) GF-5. (c) OHS. (d) ZY-1 02D.

TABLE II
COMPARISON OF SMALL SAMPLE HSIC WITH CNN-BASED METHODS

Dataset	Measure	DCNR	S³ARN	MAACNN	CapsCNN	CRCN	MR-CapsNet	Meta-RL
	OA	85.46	89.76	87.83	89.83	87.68	91.32	**95.85**
HJ-1A HSI	AA	85.85	89.82	88.44	90.44	86.43	90.75	**95.91**
	MCC	0.8225	0.8704	0.8728	0.8928	0.8577	0.8924	**0.9472**
	OA	89.12	86.88	89.88	91.03	90.13	91.78	**96.78**
GF-5 AHSI	AA	88.49	86.86	89.86	91.81	90.24	91.82	**96.57**
	MCC	0.8619	0.8788	0.8704	0.8974	0.8911	0.8909	**0.9581**
	OA	88.34	89.92	88.45	92.04	89.35	91.11	**96.13**
OHS HSI	AA	88.81	89.58	87.97	90.92	89.17	90.76	**96.42**
	MCC	0.8717	0.8773	0.8618	0.8729	0.8943	0.8841	**0.9534**
	OA	85.52	90.13	88.51	91.74	89.02	91.06	**95.99**
ZY-1 02D HSI	AA	85.74	90.48	88.16	91.31	88.96	91.24	**96.26**
	MCC	0.8508	0.8891	0.8842	0.8992	0.8713	0.9033	**0.9442**

incorporate capsule networks are a little superior to those that do not. It has been identified that CNN models are unable to capture some pixels when trained with random sampling rather than on active learning [49]. This indicates that capsule networks are able to extract a substantial amount of hidden semantic details without equally treating all bands and neighboring pixels of the HSI the same due to the multiscale convolution in capsule networks. The capsule network-based methods take advantage of increasing classification accuracy between 2% and 4% over the noncapsule network-based methods.
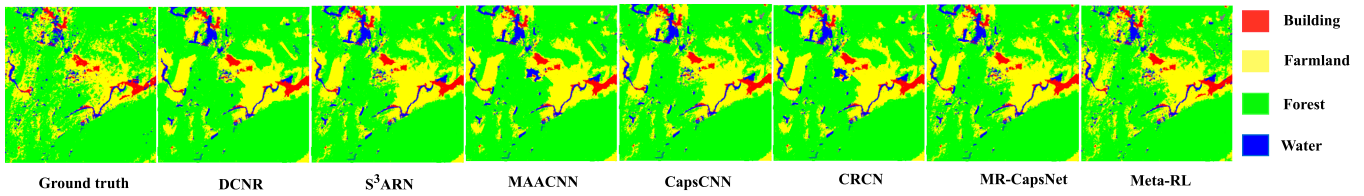
Fig. 4.   Visual effects of classification models on the HJ-1 A HSI dataset.
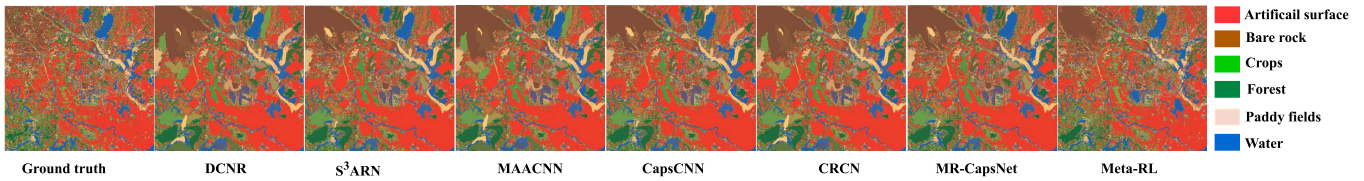

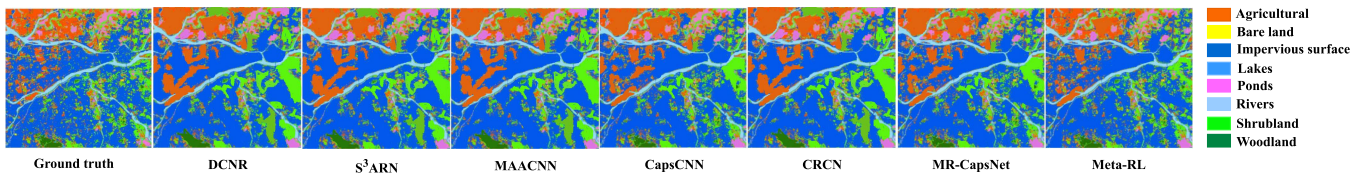Fig. 5.   Visual effects of classification models on GF-5 AHSI dataset.

Fig. 6.   Visual effects of classification models on the OHS HSI dataset.
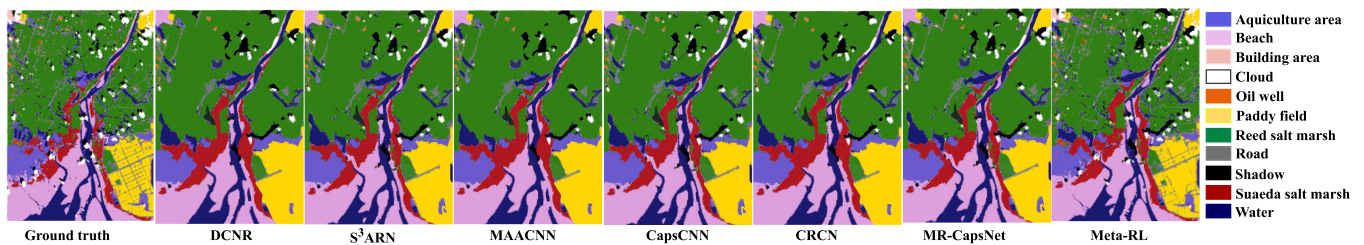

Fig. 7.   Visual effects of classification models on the ZY-1 02D HSI dataset.

Table I revealed that DCNR, among all the methods under consideration, produced the least classification performance (for all three metrics, OA, AA, and MCC). On the other hand, our method, Meta-RL, proved superior to all the methods, and this may be due to the ability of metalearning, which aids in retrieving both local and global spatial information among features with small labeled samples, while the other methods are statistical feature extraction-based retrieving typically only local feature information [2]. Fig. 4 demonstrates the visual effects of the various models on the HJ-1 A HSI dataset.

It can be observed that the Meta-RL is able to classify most of the features as compared to all the other methods since its overall visual effects are close to the ground truth. The traditional CNN method classifies most of the water, buildings, and farmlands that are scattered as forest at areas where the forest feature seems to dominate. Fig. 5 presents the visual effects of classification models on the GF-5 AHSI dataset.

The visual effects of the classification models on the GF-5 AHSI dataset are not different from the HJ-1 A HSI dataset.

This is because the characteristics of the two datasets are not much different. They have most features scattered, with a few that are clustered. However, the scattered features are dominant in the GF-5 AHSI compared to the HJ-1 A HSI dataset. It can be observed from all the models' output that Bare rock seems to appear clustered as compared to the scattered nature in the ground truth, nonetheless, Meta-RL presents less clustering effect and is able to distinguish most of the scattered features than all the other methods. Similar visual effects are realized in the visual effects of the models in Fig. 6 on the OHS HSI dataset.

The output on the Agricultural and shrubland, with scattering effects on the ground truth, seem to be clustered in all the seven classification models with Meta-RL having comparatively minimal clusters. The impervious surface having dominance seems to override most of the scattered features of lakes, ponds, shrubland, and woodland, however, rivers seem to be more obvious in all the outputs of the classification features. This suggests that the models are able to classify features with continuous effects better than scattered ones. Fig. 7 shows the visual effects of the

TABLE III
COMPARISON OF METALEARNING METHODS ON THE SMALL SAMPLE HSIC

| Dataset	Measure	MAML	SSDC	BMFSC	CMTL	MTL	CTFSL	Meta-RL
HJ-1A HSI	OA	89.46	93.76	91.83	88.83	91.68	92.32	**95.85**
	AA	89.85	93.82	92.44	89.44	90.43	91.75	**95.91**
	MCC	0.8625	0.9104	0.9128	0.8628	0.8976	0.9124	**0.9472**
GF-5 AHSI	OA	90.88	94.13	93.88	93.83	93.21	92.78	**96.78**
	AA	90.86	94.24	93.86	93.81	92.49	92.82	**96.57**
	MCC	0.9188	0.9019	0.9104	0.8604	0.9018	0.9109	**0.9581**
OHS HSI	OA	92.34	93.92	92.45	92.4	93.35	92.11	**96.13**
	AA	92.81	93.58	91.97	91.92	93.17	91.76	**96.42**
	MCC	0.9117	0.9173	0.9018	0.8518	0.9131	0.8941	**0.9534**
ZY-1 02D HSI	OA	93.02	94.13	92.51	92.46	90.52	92.06	**95.99**
	AA	92.96	94.48	92.16	92.11	89.74	92.24	**96.26**
	MCC	0.9113	0.9291	0.9242	0.8742	0.8799	0.9133	**0.9442**
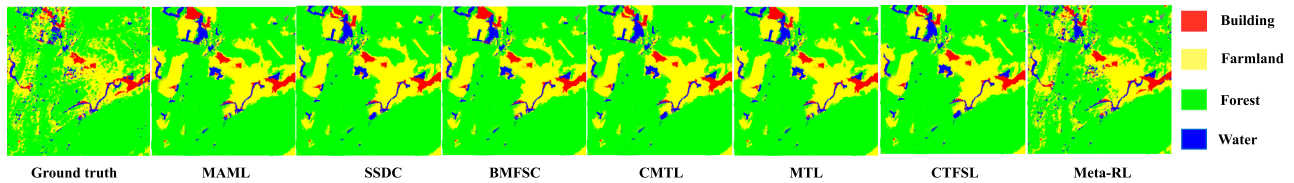
Fig. 8. Visual effects of metalearning classification models on the HJ-1 A HSI dataset.

classification models on the ZY-1 02D HSI dataset, which has slightly different characteristics with more clusters than scatters.

Unlike the Meta-RL model, the other seven models produce visual results of overriding reed salt fields dominant areas over all the other features that are scattered in such areas. Another significant output defect of the other methods compared to Meta-RL is the road features being overshadowed by the paddy fields. This follows the same limitations of the models' inability to distinguish scattered features from dominant clustered features.

B. Comparison of the Small Sample HSIC With Metalearning Methods

Existing metalearning models employed for the HSIC are compared with our model to ascertain the superiority of incorporating RL into metalearning procedures. Table III depicts the classification results of the various methods on the four selected datasets.

Unlike the traditional deep CNN approaches and the capsule network-based techniques, the metalearning methods provide quite higher classification performance, about 2%–3% overall, and an AA difference. The improvement is basically due to the reliability of metalearning models obtaining metaknowledge from similar tasks without suffering from point estimation uncertainties with small training samples [47], as well as the generalizability capabilities over other models [22]. Also, metalearning models have the ability to retrieve both discriminant and nondiscriminant in addition to informative features from target HSI [7]. The model with the least classification accuracy is found to be CMTL with the highest overall percentage accuracy of 93.83 GF-5 AHSI and least percentage accuracy of 88.83 on the HJ-1 A HSI. The MAMAL, SSDC, BMFSC, MTL, and CTFSL produced overall percentage accuracy between 90% and 95% on all the datasets under consideration. However, Meta-RL that surpasses all the models in terms of percentage accuracy

produces about 2% higher on all the datasets. In general, all the models performed comparatively well on the GF-5 AHSI and the OHS HSI datasets than the HJ-1 A HSI and the ZY-1 02D HSI datasets. Figs. 8–11 present the visual classification output of the various metalearning approaches in comparison with our method on the four datasets.

It is obvious from the visual effects from Fig. 8 that Meta-RL produces an effective classification output of the features in the HJ-1 A HSI dataset than the benchmarked metalearning methods in this study. The Meta-RL model visual result is very close to the ground truth, being able to discriminate most of the scattered building, farmland, and water features as compared to the other seven models, which cluster most of them or override the dominant forest features on the others.

On the GF-5AHSI dataset, the visual effects in Fig. 9 indicate that the CTFSL and the Meta-RL produced less scattering feature accuracy than the other methods in reference to the bare rock. On the other hand, all the models produce similar cluster effects on the crops, forest, and water. The paddy field seems to have shown the best feature classification, which may be attributed to the continuous feature representation on the dataset exhibited on the ground truth.

In the case of the OHS HSI dataset, all the metalearning approaches produce significant accurate visual effects compared to the ground truth. The only obvious variation is realized in the output of shrubland and woodland where few clusters are represented over the scattered features as shown in Fig. 10.

There is a significant improvement in the representation of road on the ZY-1 02D HSI dataset in Fig. 11 by the metalearning models compared to the traditional CNN approaches observed in Fig. 7. Nonetheless, the Meta-RL model achieved better road feature representation than the other metalearning models on the ZY-1 02D HSI dataset. This may be attributed to the effectiveness of RL on preserving the original HSI information while reducing the redundancy among spectral bands [17].
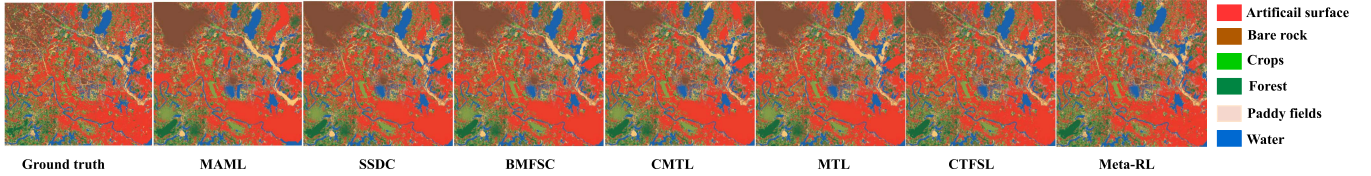
Fig. 9. Visual effects of metalearning classification models on the GF-5 AHSI dataset.
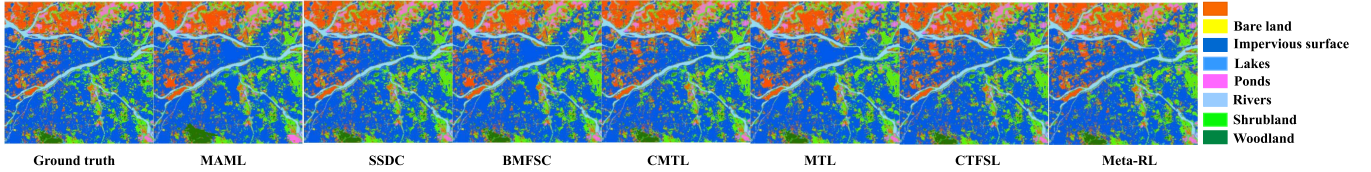

Fig. 10. Visual effects of metalearning classification models on the OHS HSI dataset.
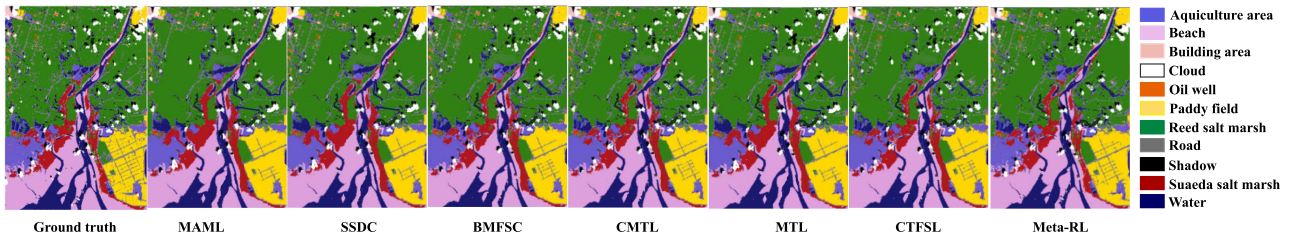

Fig. 11. Visual effects of metalearning classification models on the ZY-1 02D HSI dataset.

TABLE IV
COMPARISON OF RL AND META-RL METHODS ON THE SMALL SAMPLE HSIC

Dataset	Measure	DRLBS	RLSBS-A	MRS	Meta-RL
HJ-1A HSI	OA	92.62	**96.89**	95.15	95.85
	AA	92.23	**96.76**	96.24	95.91
	MCC	0.9187	0.9554	**0.9671**	0.9472
GF-5 AHSI	OA	93.24	96.53	96.65	**96.78**
	AA	92.96	96.21	96.34	**96.57**
	MCC	0.9075	0.955	0.9569	**0.9581**
OHS HSI	OA	93.54	96.58	**97.15**	96.13
	AA	93.66	95.83	**97.24**	96.42
	MCC	0.9219	0.9506	**0.9671**	0.9534
ZY-1 02D HSI	OA	91.85	95.32	95.74	**95.99**
	AA	92.64	95.41	96.07	**96.26**
	MCC	0.9167	0.9384	0.9382	**0.9442**

C. Comparison of Small Sample HSIC With RL and Meta-RL Methods

We consider two RL and Meta-RL approaches that have been employed in the HSIC in comparison with our proposed method. The results in Table IV indicate that RL and Meta-RL techniques are able to classify HSI much better than the traditional CNN methods as well as metalearning models.

It is worth noting that among the RL and Meta-RL methods under consideration in this study, DRLBS produced the lowest accuracy results with 93.66% AA as the highest compared to the other three that produced both overall and AA beyond 95% . The MRS method achieved the highest results of 97.24 AA on the OHS HSI dataset, while RLSBS-A led the classification accuracy on the HJ-1 A HIS dataset on OA and AA but declined in MCC. Although our Meta-RL performed poorly in relation to

the MRS and RLSBS-A methods on the two datasets, it proved superior to them on the GF-5 AHSI and the ZY-1 02D HSI datasets. This could be associated with the ability of the capsule network to effectively retrieve spectral patterns obtained at varying hierarchy levels composed as spectral-feature capsules and taking into consideration the relative spectral pattern locations and properties [14]. Figs. 12 –15 depict the visual effects of the RL and Meta-RL methods on the employed datasets.

It is obvious from the visual output in Fig. 12 that, with the exception of DRLBS, which shows some overriding clusters of forest on the other features, RLSBS-A, MRS, and Meta-RL produced results that are closer to the ground truth. Some few clusters are produced for scattered farmland features for all the models but much more significant on the DRLBS than the others on the HJ-1 HSI HSI dataset.

All the RL and Meta-RL on the GF-5 AHSI produced better visual output on artificial surface, paddy fields, and water, irrespective of the numerous scatterings on the ground truth, as evident in Fig. 13. However, significant clusters are produced on bear rock, a little on forest, and very few on crops. This indicates that RL and Meta-RL can perform well and achieve optimal classification results on this dataset with few fine-tuning processes.

The visual effects on the OHS HSI for the various Meta-RL models do not produce much variations compared to the ground truth. A few misclassifications are realized in the agricultural and shrubland features shown in Fig. 14.

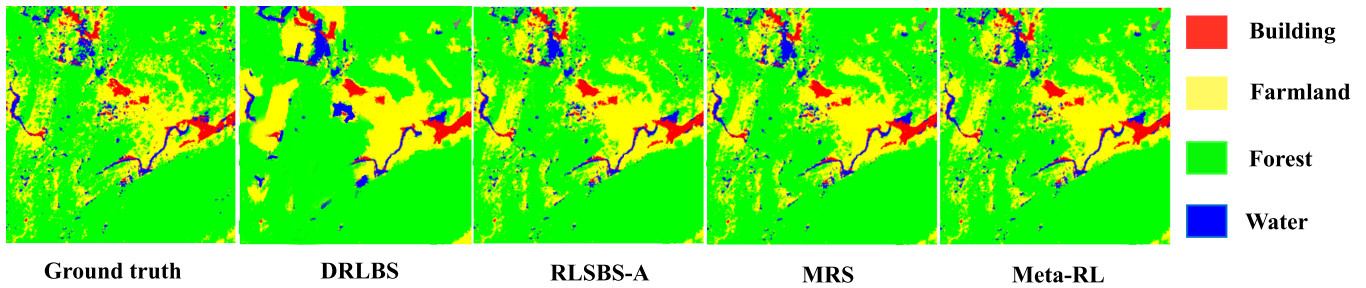There are quite a few overshadows of paddy fields on the road in the visual output of all the RL and Met-RL models on

Fig. 12. Visual effects of RL and Meta-RL classification models on the HJ-1 HSI dataset.
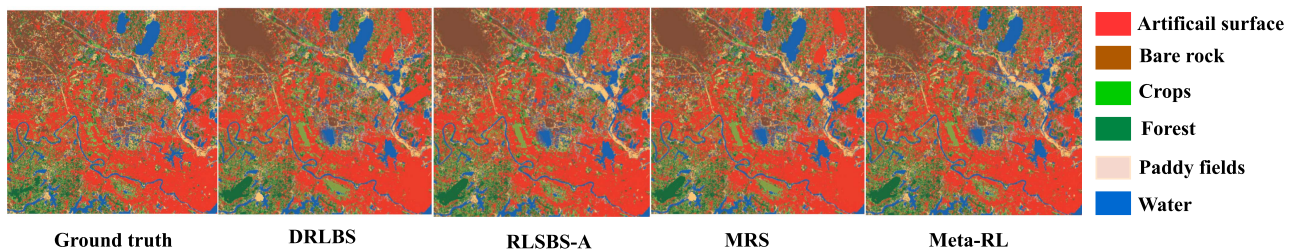

Fig. 13. Visual effects of RL and Meta-RL classification models on the GF-5 AHSI dataset.
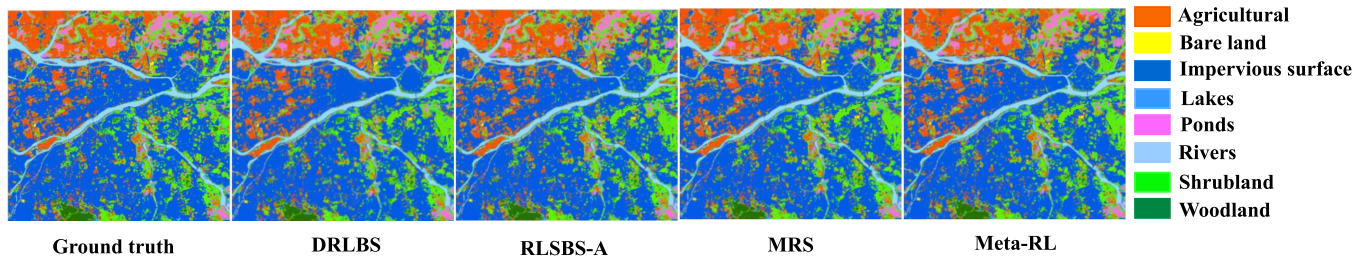

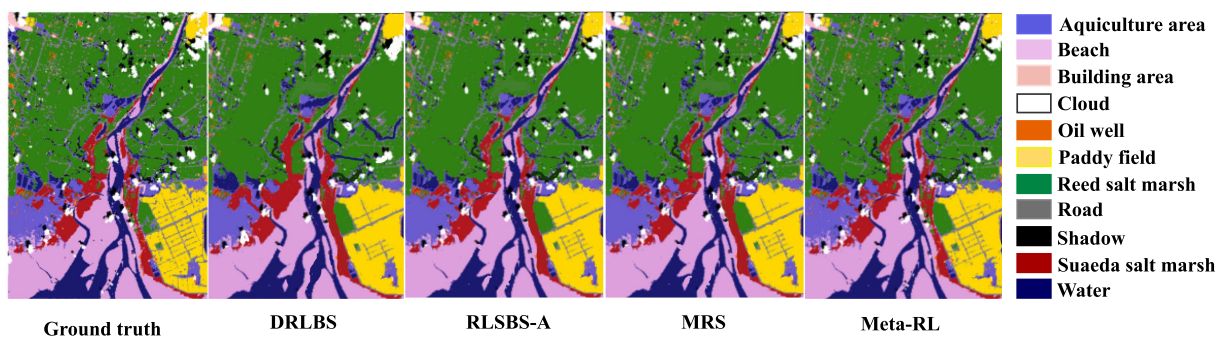Fig. 14. Visual effects of RL and Meta-RL classification models on the OHS HSI dataset.

Fig. 15. Visual effects of RL and Meta-RL classification models on the ZY-1-02D HSI dataset.

the ZY-1-02D HSI dataset; however, the Meta-RL model shows a significant difference in such output depicted in Fig. 15. It is, therefore, obvious that our model is more competitive on the four datasets than the other approaches and will be more appropriate for practical HSI small data sample classification problems. It has proven better classification results and accurate visual maps on all the datasets. It is evident that the rich abilities of the capsule network, metalearning, and RL techniques combined

are able to provide optimal classification by overcoming the drawbacks of the existing models as well as applying them individually.

D. Time Complexity Comparison of the Various Models

System acceptability highly depends on two major complexities: the functional complexity, which could be considered as the

TABLE V
COMPARISON OF TIME COMPLEXITIES OF THE VARIOUS METHODS

Datasets		CNN-based Methods			Meta-learning Methods			RL & Meta-RL Methods	
	Methods	T + V Time (s)	Testing Time(s)	Methods	T + V Time (s)	Testing Time	Methods	T + V Time(s)	Testing Time
HJ-1A HSI	DCNR	**1868.3**	17.56	MAML	3415.2	23.36	DRLBS	3996.7	23.61
	S³ARN	2867.0	24.55	SSDC	3741.6	26.60	RLSBS-A	3880.9	21.96
	MAACNN	2287.7	34.89	BMFSC	3350.4	22.46	MRS	**3657.2**	**20.83**
	CapsCNN	1921.0	24.12	CMTL	3535.2	24.19	Meta-RL	3846.0	21.57
	CRCN	2231.7	26.09	MTL	3333.6	**20.64**			
	MR-CapsNet	2376.3	**16.57**	CTFSL	**3249.6**	22.93			
	Meta-RL	3846.0	21.57	Meta-RL	3846.0	21.57			
Average Time		*2485.4*	*23.60*		*3495.9*	*23.10*		*3845.2*	*22.00*
GF-5 AHSI	DCNR	4189.7	21.34	MAML	5344.0	25.80	DRLBS	7065.0	33.71
	S³ARN	4695.7	17.95	SSDC	5969.2	24.56	RLSBS-A	6983.1	33.26
	MAACNN	4321.7	17.61	BMFSC	**4920.4**	24.98	MRS	6792.7	33.18
	CapsCNN	4508.3	19.03	CMTL	5213.2	25.30	Meta-RL	6745.4	32.98
	CRCN	4897.0	19.16	MTL	5131.6	23.66			
	MR-CapsNet	**4087.7**	**13.12**	CTFSL	5894.0	**21.72**			
	Meta-RL	6745.4	32.98	Meta-RL	6745.4	32.98			
Average Time		*4777.9*	*20.20*		*5602.5*	*25.60*		*6896.5*	*33.30*
OHS HSI	DCNR	4576.3	28.63	MAML	6535.6	37.22	DRLBS	7548.5	30.24
	S³ARN	4400.3	30.88	SSDC	6689.2	37.12	RLSBS-A	7512.7	29.53
	MAACNN	4601.7	33.63	BMFSC	5989.6	34.65	MRS	**7408.8**	**26.96**
	CapsCNN	4295.7	34.62	CMTL	6180.4	34.43	Meta-RL	7487.9	28.97
	CRCN	4775.0	**21.59**	MTL	5718.4	35.14			
	MR-CapsNet	**3731.7**	26.56	CTFSL	**5558.8**	34.73			
	Meta-RL	7487.9	28.97	Meta-RL	7487.9	**28.97**			
Average Time		*4838.4*	*29.30*		*6308.2*	*34.60*		*7489.5*	*28.90*
ZY-1 02D HSI	DCNR	2001.7	18.58	MAML	3493.2	24.70	DRLBS	3345.0	26.19
	S³ARN	**1368.3**	16.14	SSDC	3544.8	25.70	RLSBS-A	3255.0	25.58
	MAACNN	1957.7	18.62	BMFSC	3219.6	21.70	MRS	**3020.8**	24.88
	CapsCNN	1433.7	20.96	CMTL	3488.4	22.73	Meta-RL	3207.9	**24.65**
	CRCN	1459.0	**14.81**	MTL	3172.8	20.72			
	MR-CapsNet	1937.0	19.15	CTFSL	**3145.2**	**20.51**			
	Meta-RL	3207.9	24.65	Meta-RL	3207.9	24.65			
Average Time		*1909.3*	*18.99*		*3324.6*	*22.96*		*3207.2*	*25.30*

performance accuracy, and the time complexity. In this section, we evaluate the training together with validation (T+V) time, and testing time of the various models on the four datasets. Table V shows the results of the varying execution times of the models under consideration in this research.

It can be realized from Table V that fundamentally, the traditional deep CNN models have comparatively less computational cost in training, validation, and testing. This is because of the optimization concepts incorporated in the CNN methods making them robust in classification problems [50], [51].

By describing the input data at a high level of abstraction and modeling the HSI features as a set of canonical spectral–spatial patterns and their accompanying instantiation parameters, the capsule network-based models are able to reduce the computational cost. This is accomplished via the capsule network's discovery of more informative features, which reduces the complexity of the design and improves convergence [16].

Metalearning and Meta-RL models recorded comparatively higher computation time than the other models. However, the highest computational costs are found on the Meta-RL models. The high computational cost of metalearning and Meta-RL may be attributed to the increased structural complexities that may have inherent CNN and the accompanying metalearning, RL, and metareinforcement structures.

Considering the system capacity employed for the evaluation of these methods in this study, it can be said that the computational costs may be admissible, although deeper research into their implementation can provide better results. The average minimal time consumed by the models on training and validation on all the datasets is 2485.4 s obtained on the HJ-AI HSI dataset, whereas that of testing is 18.99 obtained on the ZY-1

02D HSI dataset. The lowest average computational times were on the traditional deep CNN models. Conversely, the highest computational times were recorded on the metareinforcement models with the highest average time of 7489.5 s for training and validation, and 32.7 s for testing time. Specifically, the analysis on the computational complexity of the methods on each dataset reveals the following.

1) On the HJ-1 A HSI, the DCNR model showed the least training and testing time of 1868.3 s and MR-CapsNet realized the least testing time of 16.57 s among the CNN-based methods. These results may be attributed to the fact that the DCNR has low architectural complexity since it employs a random forest classifier simplifying the model's architecture. The time efficiency of the CapsNet for testing may be as a result of the specialized nature of the network redefining the capsule units as spectra–spatial units easily adapting to new features of HSI data. The metalearning models realized CTFSL as the most computationally efficient with training and validation time of 3249.6 s and MTL leading with 20.64 s on the accounts of testing time, which can be attributed to the use of a linear classifier. Supposedly, CTFSL's reduced time complexity may be the ability of the convolutional transformer network to quickly extract local-global features to realize fast convergence. With respect to the RL and Meta-RL models, MRS showed the least computational cost of 3657.2 s on training and validation as well as testing time of 20.83 s. It is worth noting that the MRS employed a two-stage optimizer for the model, which may have contributed to the reduced exploration and exploitation time of the model. Although our model could not surpass the compared method on

computational efficiency on the HJ-1 A HSI dataset, the results obtained are below the overall average time complexities.

2) On the GF-5 AHSI dataset, MR-CapsNet maintains the lead on both training and validation as well as testing of 4087.7 and 13.12 s, respectively. The BMFSC model performed better than all the other models on training and validation consuming 4920.4 s, possibly due to the effectiveness of the variational inference approach, whereas the CTFSL maintained a lead on the testing time of 21.72 s. The proposed Meta-RL performed creditably on training and validation with 6745.4 s and achieved the most efficient testing time with 32.98 s on the RL and Meta-RL models. This can be attributed to the task encoder's ability to metatrain and test well by balancing rich temporal representation in the GF-5 AHSI data that enhanced the reduction of computational complexity.

3) Considering the computation performances of the methods on the OHS HSI dataset, MR-CapsNet proved superior with 3731.7 s on training and validation, while CRCN had the least time on testing with 21.59 s, which may be due to the effective separability of spectral similarities of spatially adjacent categories, and then, deal effectively with new diverse spatial context information. The CTFSL model maintains superiority on the metalearning models with 5558.8 s on training and validation. However, our Meta-RL had the best testing results of 28.97 s. On account of RL and Meta-RL methods, the MRS model obtained the most effective training and validation computational time as well as testing time, 7408.8 and 26.96 s, respectively.

4) The ZY-1 02D HSI dataset that recorded the least computation complexity among all the methods showed the S^3ARN as the effective method among the CNN-based methods with 1368.3 training and validation time, whereas the CRCN proved better with a testing time of 14.81 s. The effectiveness of the S^3ARN method on this dataset may be attributed to the strategy employed to fuse extracted features from multireceptive fields, which may characterize the ZY-1 02D HSI dataset, thereby, simultaneously suppressing unnecessary bands and concentrating on useful bands and adjacent pixels to speed up training. The CTFSL method consumed the least computational time on both training and validation and testing with 3145.2 and 20.51 s, respectively. The MRS method maintained the least consumer of training and validation time of 3020.8 s among the RL and Meta-RL models, while the least testing time on this dataset came from our Meta-RL model.

The computational complexity results suggest that the MRS method is significantly effective in reducing the time constraint on the classification models. However, our method performed competitively well on the account that it outperformed some of the models and the average results on all the datasets indicate higher values than our model. Hence, the competitively higher classification results promote our model to be useful in practical implementations. The promising computational output of the capsule network-based models suggests the effectiveness of their implementation. It is therefore worth noting that an appropriate structuring and fine tuning of Meta-RL with capsule network structure will improve not only classification accuracy but also computational efficiency.

VI. CONCLUSION

In this research, we have explored the benefits of supervised learning, metalearning, and RL combined in the potent method known as supervised Meta-RL. Models are given the capacity to learn from sparse data, change their behavior fast in response to new tasks, and enhance performance, which makes it extremely applicable in a variety of real-world applications. For the purpose of classifying HSIs, the integration of supervised Meta-RL with a mix of capsule networks, deep Q-learning, and task encoder networks, we employed exhibits promising potential. By utilizing the advantages of each component, this novel method has improved the classification of hyperspectral data's accuracy and effectiveness.

Further analysis of the model on computational complexity reveals less training and validation as well as testing time than the overall average time of all the benchmarked models in this study and proved competitive, especially on the testing time. This model could help with more precise and reliable classification of HSIs by learning effectively from small amounts of labeled data and applying knowledge across tasks, opening up new opportunities for applications in a variety of fields like remote sensing, agriculture, and environmental monitoring.

Validating the efficacy of this technique across various datasets and real-world circumstances will require additional study and experimentation. It is also worth emphasizing that further research will consider other appropriate techniques that will improve the classification accuracy and reduce the computational complexity such as reducing the network structure by introducing orthogonality to ensure the viability of Meta-RL in resource constraint real-time implementations.

REFERENCES

[1] S.-E. Qian, "Hyperspectral satellites, evolution, and development history," *IEEE J. Sel. Topics Appl. Earth Observ. Remote Sens.*, vol. 14, pp. 7032–7056, 2021.

[2] Y. Peng, Y. Liu, B. Tu, and Y. Zhang, "Convolutional transformer-based few-shot learning for cross-domain hyperspectral image classification," *IEEE J. Sel. Topics Appl. Earth Observ. Remote Sens.*, vol. 16, pp. 1335–1349, 2023.

[3] X. Li, Z. Li, H. Qiu, G. Hou, and P. Fan, "An overview of hyperspectral image feature extraction, classification methods and the methods based on small samples," *Appl. Spectrosc. Rev.*, vol. 58, no. 6, pp. 367–400, 2021.

[4] X. Wang, J. Liu, W. Wang, W. Chi, and R. Feng, "Weakly supervised hyperspectral image classification with few samples based on intradomain sample expansion," *IEEE J. Sel. Topics Appl. Earth Observ. Remote Sens.*, vol. 16, pp. 5769–5781, 2023.

[5] P. Ranjan and A. Girdhar, "A comprehensive systematic review of deep learning methods for hyperspectral images classification," *Int. J. Remote Sens.*, vol. 43, no. 17, pp. 6221–6306, 2022.

[6] Y. Li, L. Zhang, and L. Chen, "Spectral-spatial hyperspectral image classification based on capsule network with limited training samples," *Int. J. Remote Sens.*, vol. 43, no. 8, pp. 3049–3081, 2022.

[7] K. Gao, B. Liu, X. Yu, P. Zhang, X. Tan, and Y. Sun, "Small sample classification of hyperspectral image using model-agnostic meta-learning algorithm and convolutional neural network," *Int. J. Remote Sens.*, vol. 42, no. 8, pp. 3090–3122, 2021.

[8] Y. Wang, C. Deng, and F. Zuo, "Random augmentation pipe for hyperspectral image classification with few samples," *Int. J. Remote Sens.*, vol. 43, no. 18, pp. 6581–6604, 2022.

[9] W. Li, C. Chen, M. Zhang, H. Li, and Q. Du, "Data augmentation for hyperspectral image classification with deep CNN," *IEEE Geosci. Remote Sens. Lett.*, vol. 16, no. 4, pp. 593–597, Apr. 2019.

[10] F. Ullah et al., "Deep hyperspectral shots: Deep snap smooth wavelet convolutional neural network shots ensemble for hyperspectral image classification," *IEEE J. Sel. Topics Appl. Earth Observ. Remote Sens.*, vol. 17, pp. 14–34, 2024.

[11] Z. Mei, Z. Yin, X. Kong, L. Wang, and H. Ren, "Cascade residual capsule network for hyperspectral image classification," *IEEE J. Sel. Topics Appl. Earth Observ. Remote Sens.*, vol. 15, pp. 3089–3106, 2022.

[12] R. Lei et al., "Hyperspectral remote sensing image classification using deep convolutional capsule network," *IEEE J. Sel. Topics Appl. Earth Observ. Remote Sens.*, vol. 14, pp. 8297–8315, 2021.

[13] M. Khodadadzadeh, X. Ding, P. Chaurasia, and D. Coyle, "A hybrid capsule network for hyperspectral image classification," *IEEE J. Sel. Topics Appl. Earth Observ. Remote Sens.*, vol. 14, pp. 11824–11839, 2021.

[14] P. V. Arun, K. M. Buddhiraju, and A. Porwal, "Capsulenet-based spatial–spectral classifier for hyperspectral images," *IEEE J. Sel. Topics Appl. Earth Observ. Remote Sens.*, vol. 12, no. 6, pp. 1849–1865, Jun. 2019.

[15] J. Liu, X. Jiang, and W. Liu, "Classifying hyperspectral images with capsule network and active learning," *IEEE Int. Geosci. Remote Sens. Symp.*, pp. 3624–3627, Jul. 2022, doi: 10.1109/IGARSS46834.2022.9883239.

[16] M. E. Paoletti et al., "Capsule networks for hyperspectral image classification," *IEEE Trans. Geosci. Remote Sens.*, vol. 57, no. 4, pp. 2145–2160, Apr. 2019.

[17] L. Mou, S. Saha, Y. Hua, F. Bovolo, L. Bruzzone, and X. X. Zhu, "Deep reinforcement learning for band selection in hyperspectral image classification," Mar. 2021, *arXiv:2103.08741*.

[18] J. Feng et al., "Deep reinforcement learning for semisupervised hyperspectral band selection," *IEEE Trans. Geosci. Remote Sens.*, vol. 60, 2022, Art. no. 5501719.

[19] J. Feng, G. Bai, D. Li, X. Zhang, R. Shang, and L. Jiao, "MR-selection: A meta-reinforcement learning approach for zero-shot hyperspectral band selection," *IEEE Trans. Geosci. Remote Sens.*, vol. 61, 2023, Art. no. 5500320.

[20] A. Gupta, R. Mendonca, Y. Liu, P. Abbeel, and S. Levine, "Meta-reinforcement learning of structured exploration strategies," 2018, *arXiv:1802.07245*.

[21] Y. Wang, X. Chen, F. Wang, M. Song, and C. Yu, "Meta-learning based hyperspectral target detection using siamese network," *IEEE Trans. Geosci. Remote Sens.*, vol. 60, 2022, Art. no. 5527913.

[22] F. Zhou, L. Zhang, W. Wei, Z. Bai, and Y. Zhang, "Meta transfer learning for few-shot hyperspectral image classification," *IEEE Int. Geosci. Remote Sens. Symp.*, pp. 3681–3684, 2021, doi: 10.1109/IGARSS47720.2021.9553981.

[23] D. Pal, S. Bose, B. Banerjee, and Y. Jeppu, "Morgan: Meta-learning-based few-shot open-set recognition via generative adversarial network," in *Proc. IEEE/CVF Winter Conf. Appl. Comput. Vis.*, 2023, pp. 6295–5304, doi: 10.1109/WACV56688.2023.00623.

[24] B. Liang et al., "Few-shot aspect category sentiment analysis via meta-learning," *ACM Trans. Inf. Syst.*, vol. 41, no. 1, pp. 1–31, 2023.

[25] J. M. Kudari and S. Hembram, "Meta learning challenges and benefits," *Int. J. Eng. Res. Comput. Sci. Eng.*, vol. 8, no. 6, 2021, pp. 1–5.

[26] Y. Fu and Y. Zhang, "Reinforcement learning based plug-and-play method for hyperspectral image reconstruction," in *Proc. CAAI Int. Conf. Artif. Intell.*, 2022, pp. 466–477.

[27] L. Jiao et al., "Brain-inspired remote sensing interpretation: A comprehensive survey," *IEEE J. Sel. Topics Appl. Earth Observ. Remote Sens.*, vol. 16, pp. 2992–3033, 2023.

[28] K. Huang, W. Nie, and N. Luo, "Fully polarized SAR imagery classification based on deep reinforcement learning method using multiple polarimetric features," *IEEE J. Sel. Topics Appl. Earth Observ. Remote Sens.*, vol. 12, no. 10, pp. 3719–3730, Oct. 2019.

[29] J. Beck et al., "A survey of meta-reinforcement learning," 2023, *arXiv:2301.08028*.

[30] T. Hospedales, A. Antoniou, P. Micaelli, and A. Storkey, "Meta-learning in neural networks: A survey," *IEEE Trans Pattern Anal Mach Intell*, vol. 44, no. 9, pp. 5149–5169, Sep. 2022.

[31] Z. Ren, A. Liu, Y. Liang, J. Peng, and J. Ma, "Efficient meta reinforcement learning for preference-based fast adaptation," in *Proc. 36th Conf. Neural Inf. Process. Syst.*, 2022, pp. 1–24, doi: 10.48550/arXiv.2211.1086123.

[32] Y. Lou, J. Wu, and Y. Ran, "Meta-reinforcement learning for multiple traffic signals control," in *Proc. 31st ACM Int. Conf. Inf. Knowl. Manage.*, Atlanta, GA, USA, Oct. 17–21, 2022, pp. 4264–4268, doi: 10.1145/3511808.3557640.

[33] M. Shi, X. Zeng, J. Ren, and Y. Shi, "A multi-scale residual capsule network for hyperspectral image classification with small training samples," *Multimedia Tools Appl.*, vol. 82, pp. 40473–40501, 2023.

[34] S. Sabour, N. Frosst, and G. E. Hinton, "Dynamic routing between capsules," in *Proc. 31st Conf. Neural Inf. Process. Syst.*, 2017, pp. 1–11, doi: 10.48550/arXiv.1710.09829.

[35] R. Fakoor, P. Chaudhari, S. Soatto, and A. J. Smola, "Meta-Q-learning," in *Proc. Int. Conf. Learn. Representations*, 2020, pp. 1–17, doi: 10.48550/arXiv.1910.00125.

[36] D. Horgan et al., "Distributed prioritized experience replay," in *Proc. Int. Conf. Learn. Representations*, 2018, pp. 1–19, doi: 10.48550/arXiv.1803.00933.

[37] V. Mnih et al., "Playing Atari with deep reinforcement learning," *NIPS Deep Learn. Workshop*, pp. 1–9, 2013, doi: 10.48550/arXiv.1312.5602.

[38] L. Chunhua, Z. Xianfeng, and B. Huiyi, "Estimation of fractional vegetation cover by unmixing hj-1 satellite hyperspectral data," in *Proc. Second Int. Workshop Earth Observ. Remote Sens. Appl.*, 2012, pp. 278–281, doi: 10.1109/EORSA.2012.6261182.

[39] Y. Zhong, X. Wang, S. Wang, and L. Zhang, "Advances in spaceborne hyperspectral remote sensing in China," *Geo-Spatial Inf. Sci.*, vol. 24, no. 1, pp. 95–120, 2021.

[40] Y. Jiang, J. Wang, L. Zhang, G. Zhang, X. Li, and J. Wu, "Geometric processing and accuracy verification of Zhuhai-1 hyperspectral satellites," *Remote Sens.*, vol. 11, no. 9, 2019, Art. no. 996.

[41] W. Tan, S. Wang, H. He, and W. Qi, "Reconstructing coastal blue with blue spectrum based on ZY-1(02D) satellite," *Optik*, vol. 242, 2021, Art. no. 166901.

[42] D. Chicco and G. Jurman, "The advantages of the matthews correlation coefficient (MCC) over F1 score and accuracy in binary classification evaluation," *BMC Genomic*, vol. 21, no. 1, p. 1–3, 2020.

[43] K. Gao, B. Liu, X. Yu, and A. Yu, "Unsupervised meta learning with multiview constraints for hyperspectral image small sample set classification," *IEEE Trans. Image Process*, vol. 31, pp. 3449–3462, 2022.

[44] T. Li, J. Leng, L. Kong, S. Guo, G. Bai, and K. Wang, "DCNR: Deep cube CNN with random forest for hyperspectral image classification," *Multimedia Tools Appl.*, vol. 78, no. 3, pp. 3411–3433, 2018.

[45] H. Zhang, J. Yao, L. Ni, L. Gao, and M. Huang, "Multimodal attention-aware convolutional neural networks for classification of hyperspectral and LiDAR data," *IEEE J. Sel. Topics Appl. Earth Observ. Remote Sens.*, vol. 16, pp. 3635–3644, 2023.

[46] X. Zhang et al., "Spectral-spatial distribution consistent network based on meta-learning for cross-domain hyperspectral image classification," *IEEE Trans. Geosci. Remote Sens.*, vol. 61, 2023, Art. no. 5520915.

[47] J. Zhang, L. Liu, R. Zhao, and Z. Shi, "A Bayesian meta-learning-based method for few-shot hyperspectral image classification," *IEEE Trans. Geosci. Remote Sens.*, vol. 61, 2023, Art. no. 5500613.

[48] Y. Cheng, W. Zhang, H. Wang, and X. Wang, "Causal meta-transfer learning for cross-domain few-shot hyperspectral image classification," *IEEE Trans. Geosci. Remote Sens.*, vol. 61, 2023, Art. no. 5521014.

[49] Z. Shu, Z. Liu, J. Zhou, S. Tang, Z. Yu, and X.-J. Wu, "Spatial–spectral split attention residual network for hyperspectral image classification," *IEEE J. Sel. Topics Appl. Earth Observ. Remote Sens.*, vol. 16, pp. 419–430, 2023.

[50] P. Maji and R. Mullins, "On the reduction of computational complexity of deep convolutional neural networks," *Entropy*, vol. 20, no. 4, 2018, Art. no. 305.

[51] J. Ephrath, M. Eliasof, L. Ruthotto, E. Haber, and E. Treister, "LeanConvNets: Low-cost yet effective convolutional neural networks," *IEEE J. Sel. Topics Signal Process.*, vol. 14, no. 4, pp. 894–904, May 2020.

Prince Yaw Owusu Amoako received the bachelor's degree in computer science from Valley View University, Accra, Ghana, in 2005, and the Master of Philosophy degree in computer engineering from the Kwame Nkrumah University of Science and Technology, Kumasi, Ghana, in 2011. He is currently working toward the Ph.D. degree in computer science and technology with the Nanjing University of Science and Technology, Nanjing, China.

He is currently a Lecturer with Valley View University. His research interest include machine learning, hyperspectral image processing, and educational technologies

Guo Cao (Member, IEEE) received the Ph.D. degree in pattern recognition and intelligence system from Shanghai Jiao Tong University, Shanghai, China, in 2006.

Since 2007, he has been with the School of Computer Science and Engineering, Nanjing University of Science and Technology, Nanjing, China, where he is currently a Full Professor. During 2012–2013, he was a Visiting Scholar with the Department of Radiology, University of Chicago, Chicago, IL, USA. From 2016 to 2017, he was a Visiting Scholar with the Department of Geography, University of Florida, Gainesville, FL, USA, where he focused on change detection. His research interests include machine learning and remote sensing image processing.

Yuexuan Wang received the B.Sc. degree in electronic information science and technology from the School of Physics and Information Technology, Shaanxi Normal University, Xi'an, China, in 2017, and the Ph.D. degree in control science and engineering from the School of Computer Science and Engineering, Nanjing University of Science and Technology, Nanjing, China, in 2018.

Her research interests include medical image processing and deep learning.

Di Yang received the Ph.D. degree in geography from the University of Florida, Gainesville, FL, USA, in 2019.

He is currently an Assistant Professor with the Wyoming Geographic Information Center (WyGISC), University of Wyoming, Laramie, WY, USA. He is also a Geographer and Programmer focusing on the study of human–environment interactions by using remote sensing imageries. He is a bridge builder for closing the gap between the operational uses of scientific remote sensing and GIS techniques and land management practices at the regional scale.

Qiqiong Yu received the M.S. degree in applied mathematics from the Nanjing University of Information Science and Technology, Nanjing, China, in 2017. She is currently working toward the Ph.D. degree in computer science and technology with the School of Computer Science and Engineering, Nanjing University of Science and Technology, Nanjing.

Her research interests include image processing, pattern recognition, and machine learning.

Lord Amoah received the B.S. degree in computer science, in 2018, from Valley View University, Accra, Ghana, and the M.Sc. degree in computer science and technology, in 2021, from the School of Computer and Software, Nanjing University of Information Science and Technology, Nanjing, China, where he is currently working toward the Ph.D. degree in information security with the School of Computer and Software.

His research interests include reversible data hiding, digital image processing, and information security.